www.sciencemag.org/cgi/content/full/1120941/DC1

Supporting Online Material for

The Ste5 Scaffold Allosterically Modulates Signaling Output of the Yeast Mating Pathway

Roby P. Bhattacharyya, Attila Reményi, Matthew C. Good, Caleb J. Bashor, Arnold M. Falick, Wendell A. Lim*

*To whom correspondence should be addressed. E-mail: lim@cmp.ucsf.edu

Published 19 January 2006 on *Science* Express
DOI: 10.1126/science.1120941

This PDF file includes:

Supporting Online Material

1. Materials and methods
2. Supporting figures, Fig. S1 – S9
3. Supporting tables, Tables S1 – S3
4. Supporting references

Materials and Methods:

Constructs and strains:

Plasmids used in this study are shown in **Table S1**. For yeast expression, Ste7 and Ste5 were cloned from *S. cerevisiae* genomic DNA along with 500 or 1000 bp of upstream sequence to encompass their native promoters into low-copy yeast vectors (pRS314 for Ste7, pRS316 for Ste5). For bacterial expression, the Fus3 ORF was cloned from *S. cerevisiae* genomic DNA into a pET19b-based vector for His-tagged protein expression. GST fusion peptides were cloned by oligonucleotide annealing or PCR into pGEX4T-1 or a pET19b-based vector with the GST sequence from pGEX inserted. The cDNA of ΔNSte5 ($Ste5^{280-917}$) was cloned into a pET19b expression vector encoding a fusion protein with an N-terminal GST- and a C-terminal 6xHis tag. Mutations were made by standard two-step PCR mutagenesis techniques (except as noted below) and verified by DNA sequencing.

Yeast strains used in this study are shown in **Table S2**. Gene knockouts were made using standard gene disruption techniques.

Protein expression and purification:

Expression and purification of recombinant Fus3 is described elsewhere (*S1*). Tyrosine phosphorylated Fus3 (Fus3-pY) was produced by incubating non-phosphorylated Fus3 (Fus3-np) with 2mM ATP in the presence of 5 mM $MgCl_2$ and saturating amount of Ste5_pep overnight at room temperature. The sample was then loaded on a gel filtration column in 20 mM Tris pH=8.0, 1M NaCl, 10% glycerol, 2mM DTT to separate the kinase and activator. Dual-phosphorylated Fus3 (Fus3-pYpT) was produced by incubating Fus3-np with ΔNSte5 ($Ste5^{280-917}$) and $Ste7^{S359E,T363E}$ (expressed and purified as described (*S1*)) in kinase buffer (20 mM Tris pH=8.0, 100mM NaCl, 10% glycerol, 5mM $MgCl_2$, 2mM TCEP, 2mM ATP) overnight at room temperature. The reaction mix contained these three proteins in 30:3:1 molar ratio, respectively. Fus3 was separated from the scaffold, kinase activator and ATP by ion-exchange. Phosphorylation states of Fus3 were confirmed by mass spectrometry and isoelectric focusing.

GST-peptides were expressed in Rosetta(DE3)pLysS cells at 37 °C, protein production was induced with the addition of 1mM IPTG. Cells were harvested after 3 hours and lysed in PBS + 2mM DTT by sonication. For activation assays GST-peptides were eluted with GSH elution buffer (60mM Tris pH=8.0, 150 mM NaCl, 10% glycerol, 2mM DTT, 15 mM reduced glutathione), concentrated and directly used for Fus3 activation studies.

ΔNSte5 protein production was induced in Rosetta(DE3)pLysS cells at 25 °C for 5 hours with the addition of 100 mM IPTG. ΔNSte5 was first purified on Ni-NTA

agarose by standard procedures and the eluted sample was loaded onto a GST-column, washed with 20mM Tris pH=8.0, 150 mM NaCl, 10% glycerol, 2mM DTT and finally eluted in GSH elution buffer (60mM Tris pH=8.0, 150 mM NaCl, 10% glycerol, 2mM DTT, 15 mM reduced glutathione). To generate the activation deficient form of ΔNSte5 protein ($\Delta NSte5^{ND}$), the DNA of the wild-type protein was mutated by using the Transformer Site-Directed Mutagenesis Kit (Clontech) and the protein expressed and purified as described above.

MBP was purchased from Sigma (M1891).

Peptide synthesis, labeling, and purification:

Free peptides for crystallography and fluorescence anisotropy studies were chemically synthesized with an ABI433A Peptide Synthesizer (Applied Biosystems) using the FastMoc protocol at 0.1 mmol scale. For crystallography, Ste5_pep contained amino acids 287-316: *N*-Ac-TPVERNQTIPSQAPSLNPNLILAPPKERN-$CONH_2$-*C*. For fluorescence anisotropy, a longer version of Ste5_pep (amino acids 280-321: *N*-Ac-PPFGLSY**TPVERNQTIPSQAPSLNPNLILAPPKERN**QIPQKKC-$CONH_2$-*C*) was synthesized with a Cys residue appended at the C-terminus for labeling. For competition fluorescence anisotropy, Ste5_pep and a version of Ste5_pep with a three amino acid insertion in the linker region ($Ste5\_pep^{L+3}$: *N*-Ac-TPVERNQTIPSQAPS**SSS**LNPNLILAPPKERN-$CONH_2$-*C*) was synthesized. For in vivo studies, we synthesized alpha factor pheromone (*N*-WHWLQLKPGQPMY-*C*). All peptides were purified by reverse-phase chromatography on a C-18 column (Vydac)

using a Dynamax high pressure liquid chromatography (HPLC) system and verified by matrix-associated laser desorption and ionization (MALDI) mass-spectrometry using a Voyager-DE STR BioSpectrometry Workstation (Applied Biosystems). The peptide to be labeled was treated with fluorescein using the thiol-reactive 5-iodoacetamidofluorescein reagent (Molecular Probes) according to protocols provided by the supplier. Fluoresceinated peptide was HPLC purified again after labeling to remove the unreacted fluorophore, and labeling was verified by MALDI.

Peptide binding experiments:

Bacterial lysates containing GST-peptides were loaded to glutathione agarose (Sigma), washed three times with PBS + 2mM DTT and incubated with the prey in binding buffer (20mM Tris pH 8.0, 150 mM NaCl, 0.05% IGEPAL, 2mM TCEP) for 30 minutes at 4 °C. The beads were then washed three times with binding buffer and resuspended in SDS sample buffer (50 μl). 10 μl of each sample was used for SDS-PAGE and protein bands were visualized by Coomassie staining. In a typical pull-down experiment 10 μl of glutathione resin saturated with GST-tagged bait was used and incubated in 200 μl of binding buffer containing 10 μM prey (Fus3).

Binding affinities for Fus3/Ste5_pep and Ste5_pep^{L+3} binding were measured by monitoring peptide fluorescence polarization change upon MAPK binding. Fluorescence polarization was measured at different concentrations of purified Fus3 with an Analyst AD & HT Detection System (LJL Biosystems) plate reader in 384 well-plates (Excitation: 485 nm, Emission: 540 nm). The fluoresceinated peptide, the extended

version of Ste5_pep (amino acids 280-321), was present at 10 nM in 20 mM TrisCl pH 8.0, 100 mM NaCl, 5 mM DTT and 1 mg/ml BSA. The resulting binding isotherms were fit to a quadratic binding equation using ProFit 5.1.0 (Quantum Soft) as described elsewhere (*S2*). The Kd for the fluorescein-labeled extended version of Ste5_pep (1.7 μM) was then used for determining binding affinities for unlabelled Ste5_pep and Ste5_pep^{L+3} (287-TPVERNQTIPSQAPSLNPNLILAPPKERNQ-316 and TPVERNQTIPSQAPSSSSLNPNLILAPPKERNQ, respectively). Fluorescence polarization was monitored in triplicate at constant concentrations of Fus3 and different concentrations of unlabeled peptides in a competition binding experiment. K_ds for unlabeled peptide binding were then determined by fitting fluorescence polarization data obtained at different concentrations of unlabeled peptide to a competition binding equation (*S2*).

Crystal structure determination:

Crystallization trials were carried out at 20 °C by using the vapor diffusion hanging drop method. Protein samples for crystallization contained 20mM Tris pH 8.0, 100 mM NaCl, 10% glycerol, 2mM TCEP, 2mM $MgCl_2$ and 2mM ATP-γS. Starting protein concentration was 8 mg/ml. Fus3^{VF} is a non-phosphorylatable form of Fus3 where Thr180 and Tyr182 were mutated to valine and phenylalanine, respectively. Since recombinant Fus3 is partially phosphorylated at the activation segment, use of this mutant facilitated Fus3 sample preparation. Note that the crystal structures of Fus3^{VF} and non-phosphorylated wild-type Fus3 (Fus3-np) are identical (*S1*).

Highest diffraction quality crystals for Fus3-pY grew from well-solutions containing 25-28% PEG1000, 0.1M MES pH 6.1, 5-10% MPD in one or two days. The crystals belong to the space group ($P2_12_12_1$) with cell dimensions: a = 56.8 Å, b = 62.5 Å, c = 86.0 Å.

Fus3/Ste5_pep complex was formed by mixing $Fus3^{VF}$ protein with chemically synthesized peptide in 1:2 molar ratios. The length of the peptide used in the crystallization trials was systematically varied. The best crystals were obtained with a 30-mer peptide (287-TPVERQTIYSQAPSLNPNLILAAPPKERNQ-316). Binary protein-peptide complexes were grown in a solution containing 18% PEG3350, 0.1M Mes pH 6.1, 10% MPD and 0.2M KSCN. The complex crystals belong to space group $P2_12_12_1$ with cell dimensions a = 94.62 Å, b = 95.21 Å, c = 101.66 Å. Crystals could be also grown in the absence of Ste5_pep under the same crystallization conditions. These crystals belong to the same space group but with different cell dimensions: a = 79.15 Å, b = 94.47 Å, c = 113.2 Å. Single crystals were soaked in well-solution supplemented with 25% (v/v) glycerol, then mounted on nylon loops and flash-frozen in liquid nitrogen prior to data collection at 100 K. Datasets were collected at beamline 8.3.1 of the Advanced Light Source, Lawrence Berkeley National Laboratory. Data reduction and scaling was done using the HKL package (*S3*).

Crystal structure of Fus3-pY was solved with molecular replacement with AMoRe (*S4*) using the structural model of Fus3-np as the search model. Similar to the crystals of $Fus3^{VF}$ and Fus3-np grown under similar conditions (*S1*), the rotation and translation search as well as crystal water content indicated the presence of one Fus3

molecule in the asymmetric unit. Structural models of Fus3-np and Fus3^{VF} contain a full-length molecule of Fus3 (1-353) interspersed with an invisible segment encompassing the activation loop (164-179). In the Fus3-pY structure, electron density is missing for a larger region: from residue 164 till 184. This structure also contains an ADP nucleotide in complex with one Mg^{2+} ion.

Molecular replacement was also used to solve the structure of Fus3^{VF} as well as the Fus3^{VF}/Ste5_pep complex under a different crystallization condition containing 0.2 M KSCN. Coordinates of Fus3^{VF} (*S1*) were used as the search model in AMoRe. The rotation function, for data between 8 and 3.5 Å resolution, indicated two apparent solutions for both crystals. The translation search was applied to one of the solutions, giving an R factor of 52.9% for Fus3^{VF} and 53.4% for Fus3^{VF}/Ste5_pep. Next, these solutions were fixed and new translation searches were carried out using the other rotation function solution. The R factors dropped to 49.5 % (Fus3^{VF}) and 49.3% (Fus3^{VF}/Ste5_pep). The final molecular replacement models contain two Fus3 molecules in the asymmetric unit for both the Fus3^{VF} and Fus3^{VF}/Ste5_pep complex. The solutions after rigid body refinement in AMoRe had an R factor of 48.0 % and 48.4 %, for data between 8 and 3.5 Å resolution, respectively.

Model building was performed with O (*S5*) and the structure was refined using CNS (*S6*) interspersed with manual model building. After locating both Fus3 molecules in the asymmetric unit, the non-crystallographic symmetry (NCS) axis was derived by overlaying the two MAPK molecules. NCS information was used only in the initial phases of the structure refinement. Electron density for Ste5_pep was clearly

interpretable after some initial rounds of refinement and its structural model was manually built in O.

The final two models of Fus3 contain the full-length model of the protein apart from residues 164-179. This region appears to be flexible and not visible in the electron density map. 20 amino acids of Ste5_pep could be located in the electron density map. An eight amino acid long region (APSLNPNL), which links Site A (PVERQTIYSQ) and Site B (ILAAPPKERN) together, has no interpretable electron density and therefore it is likely to be flexible. The $Fus3^{VF}$ and $Fus3^{VF}$/Ste5_pep complex crystals do not show interpretable electron-density in the nucleotide binding pocket, so nucleotide co-factors were not included in the final structural models.

Statistics of the refinement for $Fus3^{VF}$, $Fus3^{VF}$/Ste5_pep complex and Fus3-pY are listed in **Table S3**.

Kinase assays:

MAPK activity was measured in kinase assays. Depending on the experiment, the enzyme (2 μM) was incubated with activator peptides as free peptides or GST-fusions (50 μM), or longer proteins GST-ΔNSte5 or GST-$\Delta NSte5^{ND}$ (1 μM) in 100 μl of kinase reaction buffer (20 mM Tris pH=8.0, 150 mM NaCl, 0.05% IGEPAL, 2mM TCEP, 2mM $MgCl_2$). For peptide activation experiments, free peptides showed slightly higher activation than equivalent GST fusions (50-fold vs. 40-fold rate enhancements). MBP concentration was 50 μM, and samples also contained 0.5 mM ATP and 5 μM radioactively labeled $ATP^{32}(\gamma)$. 10 μl aliquots of the reaction mix were taken at different

time points and the reaction was stopped by the addition of 4xSDS sample buffer. Samples were run on SDS-PAGE and gels were dried. After gel exposure to a phosphoimager screen, radioactivity of substrate protein bands were quantified by scanning in a Typhoon 8600 instrument (Molecular Dynamics, Amersham Pharmacia Biotech) and analyzed using Image Quant 5.1 software (Molecular Dynamics, Amersham Pharmacia Biotech). Data were fit using ProFit software (Quantum Soft) to either a first-degree polynomial for the initial, linear phase of ^{32}P incorporation or, if saturation was approached in autophosphorylation reactions, to an equation describing unimolecular reaction kinetics: $y(t) = A_{min} + A_{max}*(1 – \exp(-k*t)$, where y = ^{32}P counts, A_{min} = ^{32}P counts at t = 0, A_{max} = ^{32}P counts at saturation, k = reaction rate, and t = time. In the latter case, A_{max} for slower reactions was fixed to the fitted value from reactions that approached saturation (i.e., with Ste5_pep present).

Mass spectrometry:

Mass measurements on intact proteins were made on a Model 3000 Bruker-Agilent Esquire quadrupole ion trap mass spectrometer (Bruker Instruments, Billerica, MA) with electrospray ionization. Prior to determining its mass spectrum, each protein was desalted by microbore reversed-phase high-performance liquid chromatography. A microprotein analyzer HPLC (Michrom Bioresources, Inc., Auburn, CA) was used to elute approximately 10 ug of the full-length protein from a Polymer Labs PLRP column (300A pore size, 1 x 150 mm) using a 10-50% acetonitrile gradient in water with 0.1%

TFA over 7 min at 0.75 mL/min. MS data were acquired on approximately 1 uL of the collected eluent.

Approximately 0.1-0.5 pmol of each digest was desalted with a C18 ZipTip (Millipore, Billerica, MA). Then approximately 0.5 uL of the resulting solution was mixed with an equal volume of matrix solution and allowed to dry on the MALDI target. The matrix solution used was a 10 g/L solution of alpha-cyano-4-hydroxycinnamic acid in 50% acetonitrile/50% 0.1% aqueous TFA. All mass spectrometric measurements on peptides were performed on an Applied Biosystems (Foster City, CA) 4700 Proteomics Analyzer, a tandem time-of-flight instrument (TOF/TOF) with a MALDI ion source (*S7*). Normal reflector spectra were acquired first to verify the masses of the peptides of interest. External calibration using known peptide standards was used, typically giving masses to better than 50 ppm accuracy. MS/MS CID spectra were acquired on each peptide of interest, using air as the collision gas and 1 keV (lab frame) collision energy. Default calibration of the mass scale was used for all MS/MS spectra, which typically provided fragment masses accurate to <0.1 Da. Interpretation of the spectra was done manually.

Flow cytometry:

For flow cytometric analysis of GFP expression from the Fus1 promoter, cultures of either CB011 or CB006Δste5 (for Ste5 plasmids) or MG40 (for Ste7 plasmids) were treated in early log phase with pheromone (alpha factor) from 0.1 to 200 nM for either 110 minutes (for Ste5 alleles) or 120 minutes (for Ste7 alleles) and analyzed on a BD

LSR-II flow cytometer (BD Biosciences) after brief sonication at low power to disrupt cell clumps. 10,000 cells were counted for each reading, and GFP fluorescence was measured by exciting at 488 nm with a 20 mW Coherent Sapphire argon ion laser and detecting emission on the FITC channel using 515-545 nm filters.

Fluorescence measurements at long time points (> 2 hours) were complicated by pheromone-induced cell cycle arrest and associated increase in cell volume. To avoid this complication, measurements were either made at early time points or in *far1*Δ strains that uncouple cell cycle arrest from mating response (*S8*). Similar results were observed in both cases. All flow cytometry experiments were performed in *bar1*Δ strains that lack the protease that degrades alpha factor (*S9*).

The resulting data were analyzed using FlowJo analysis software (TreeStar, Inc.). Cell populations were gated based upon forward scatter (a rough measure of cell size) and fluorescence to include only intact single cells and exclude cell clumps and cell fragments generated by sonication. After pheromone treatment, a corresponding population of cells shifted along the FITC axis to higher fluorescence at the same forward scatter. The gate used for data analysis in the absence of alpha factor was allowed to re-center on the treated population using the "magnetic gate" feature of the FlowJo software. Mean cellular fluorescence was calculated for this gated population, and the resulting dose-response data were fit using ProFit software (Quantum Soft) to a Hill equation: $F(a) = F_{min} + (F_{max} - F_{min})*a^{(n_H)}/(C_m^{(n_H)} + a^{(n_H)})$, where F = mean fluorescence, a = concentration of alpha factor, F_{min} = mean fluorescence with no alpha factor, F_{max} = mean fluorescence with saturating alpha factor, C_m = concentration of alpha factor at which

fluorescence is half-maximal, and n_H = Hill coefficient. Consistent with previous reports (*S10*), Fus1-GFP showed a unimodal, approximately Gaussian distribution at all doses of alpha factor, indicating a graded response to pheromone stimulus.

Data shown are from single dose-response experiments that are representative of many replicates. Experiments carried out on three independent transformants matched very closely (**Fig. S7**); error bars for mean fluorescence values (**Fig. 4-5**) are estimated to be smaller than the data symbols.

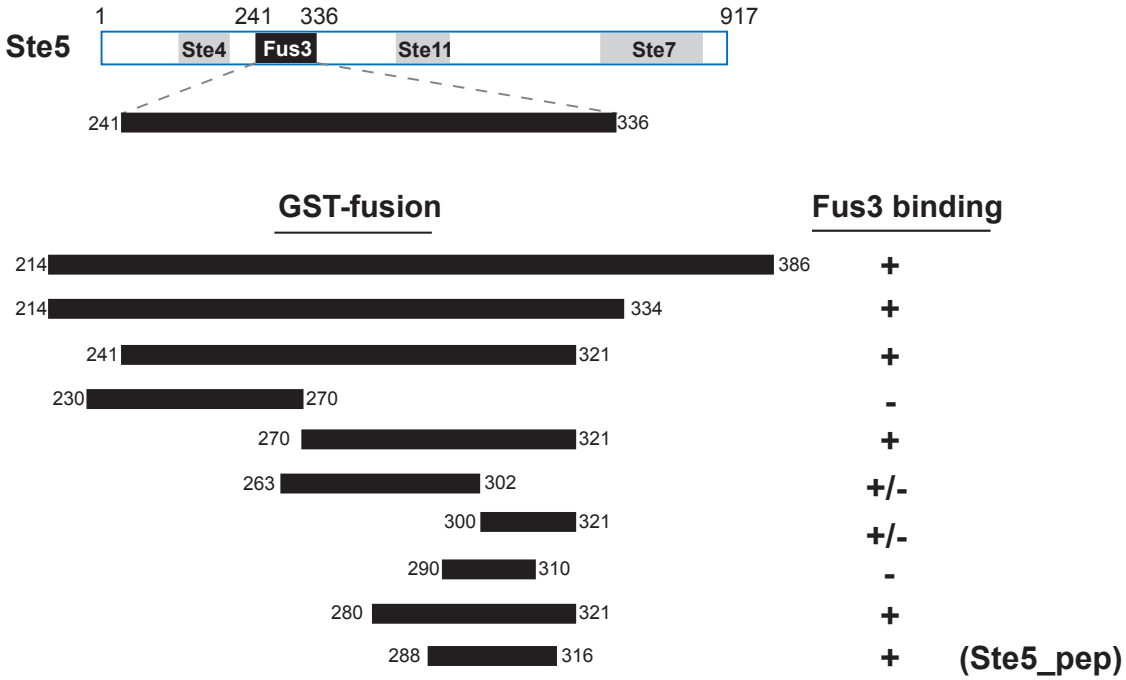

Figure S1. Mapping minimal Fus3 binding region in Ste5 by GST pulldown.
A series of GST fusion constructs was generated as shown, starting from an expanded version of the Fus3 binding region of Ste5 mapped by yeast two-hybrid studies (*S11*). We mapped the Fus3 binding element within this region to a minimal peptide from amino acids 288 to 316, which we refer to as Ste5_pep. In some experiments, a slightly extended version of Ste5_pep is used (amino acids 280-321).

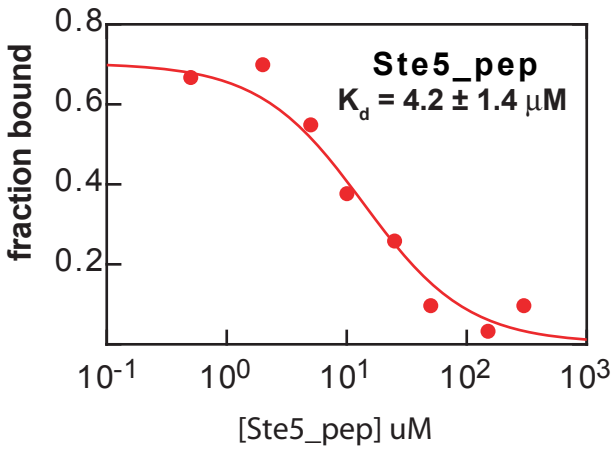

Figure S2. Measuring Ste5_pep binding affinity for Fus3 by competition fluorescence polarization.
Unlabeled Ste5_pep (amino acids 287-316) was added at varying concentrations to compete with a constant level of fluoresceinated Ste5_pep (amino acids 280-321) for binding to a constant level of $Fus3^{T180V,Y182F}$, and the fluorescence polarization of the fluoresceinated species was monitored. The resulting K_d was similar to that for other Fus3 binding peptides (*S1*).

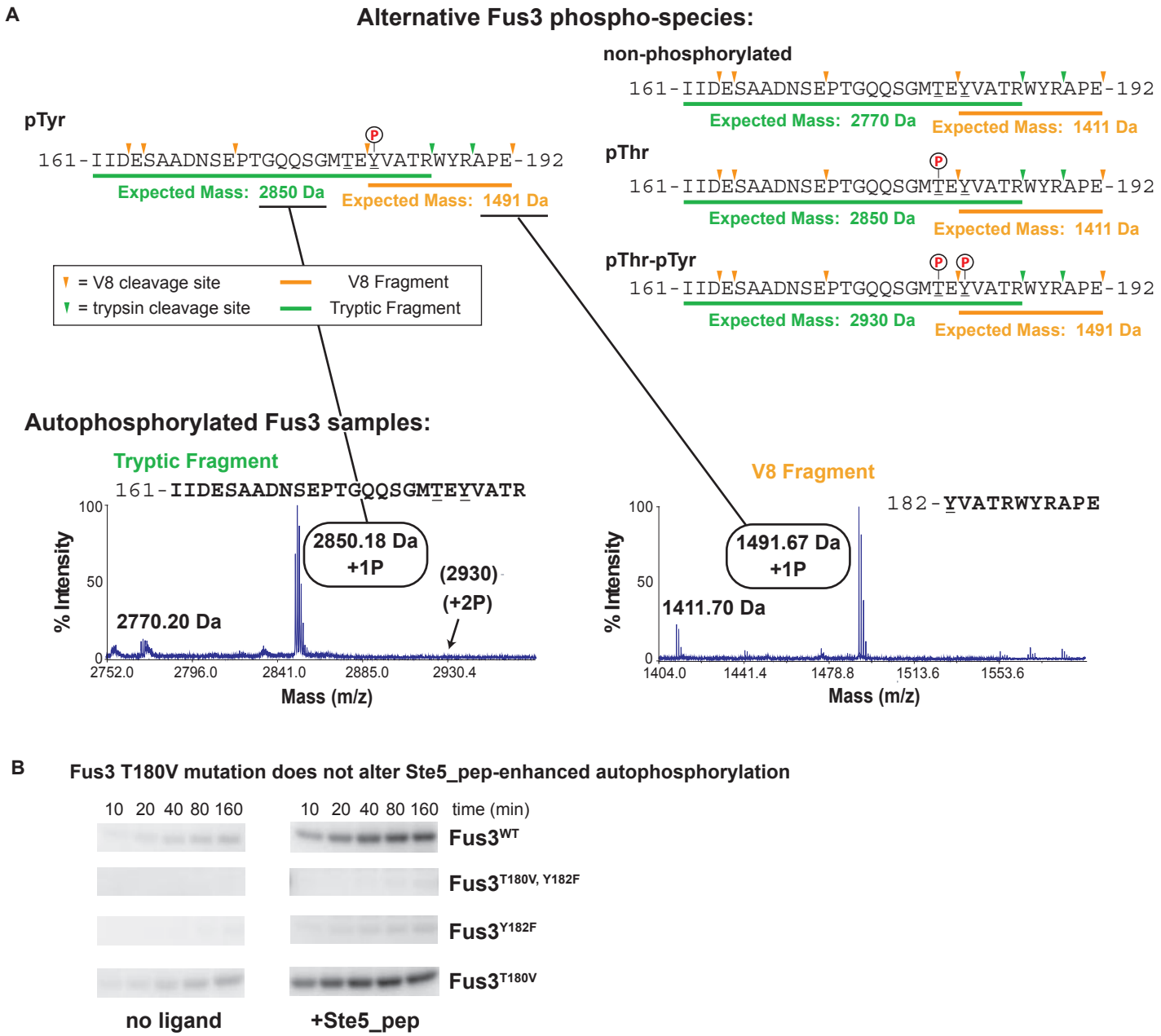

Figure S3. Fus3 activated by Ste5_pep is monophosphorylated on Tyr182 in the activation loop. **(A)** Mass spectrometry evidence. Electrospray ionization of full-length Fus3 after autoactivation in the presence of Ste5_pep revealed only singly phosphorylated Fus3 and trace amounts of unphosphorylated Fus3, but no dually phosphorylated Fus3 (*S12*). Proteolytic mapping followed by MALDI is consistent with a single phosphate on Tyr182, but not Thr180 (the other activation loop phosphoacceptor). Top panels show Fus3 cleavage products near the activation loop, along with expected masses for each of the four possible combinations of activation loop phosphorylation. Bottom panels show MALDI spectra for relevant fragments from trypsin and V8 cleavage. Only the pTyr species is consistent with both spectra. Analysis of peptide fragmentation of the V8 fragment by MS/MS verified that the single phosphate is present on Tyr182 and not Thr185, the only other phosphorylatable residue in both peptides (S*12*). **(B)** Biochemical evidence. Mutation of Tyr182, but not Thr180, prevents autophosphorylation in the presence or absence of Ste5_pep. Autoradiograms show ^{32}P incorporation into bacterially expressed, phosphatase-pretreated Fus3 variants. Furthermore, autoactivated Fus3 is recognized by anti-pTyr antibodies, but not anti-pSer/Thr antibodies (S*13*).

CONCLUSION: Fus3 autoactivated in the presence of Ste5_pep is singly phosphorylated on Tyr182, one of two phosphoacceptors in the activation loop.

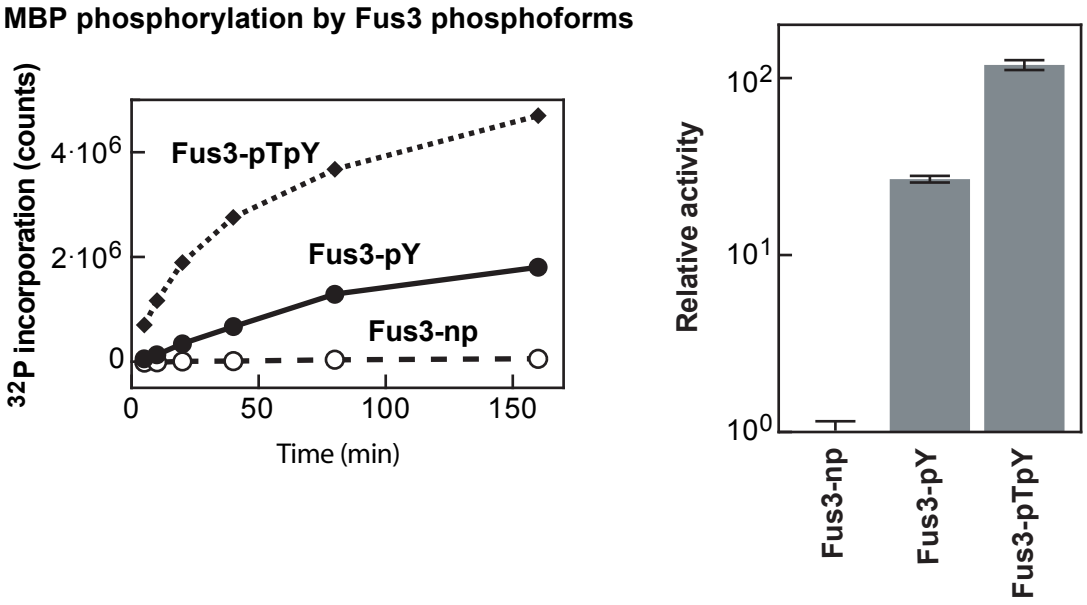

Figure S4. Relative activity of doubly, singly, and non-phosphorylated forms of Fus3. Phosphorylation of Fus3 on its activation loop enhances its kinase activity. Myelin basic protein (MBP) was incubated with Fus3 that was either non-phosphorylated (Fus3-np: open circles, dashed line), singly phosphorylated on Tyr182 (Fus3-pY: filled circles, solid line), or dually phosphorylated on Thr180 and Tyr182 (Fus3-pTpY: filled diamonds, dotted line). MBP phosphorylation data from an autoradiogram was quantified and plotted (left panel), and relative initial rates of ^{32}P incorporation into MBP were plotted on a logarithmic scale (right panel).

CONCLUSION: Tyrosine phosphorylation alone increases kinase activity by a factor of 25 over the non-phosphorylated state, while additional threonine phosphorylation yields a further 5-fold increase in kinase activity (dually phosphorylated Fus3 is more active by a factor of 120 than non-phosphorylated Fus3).

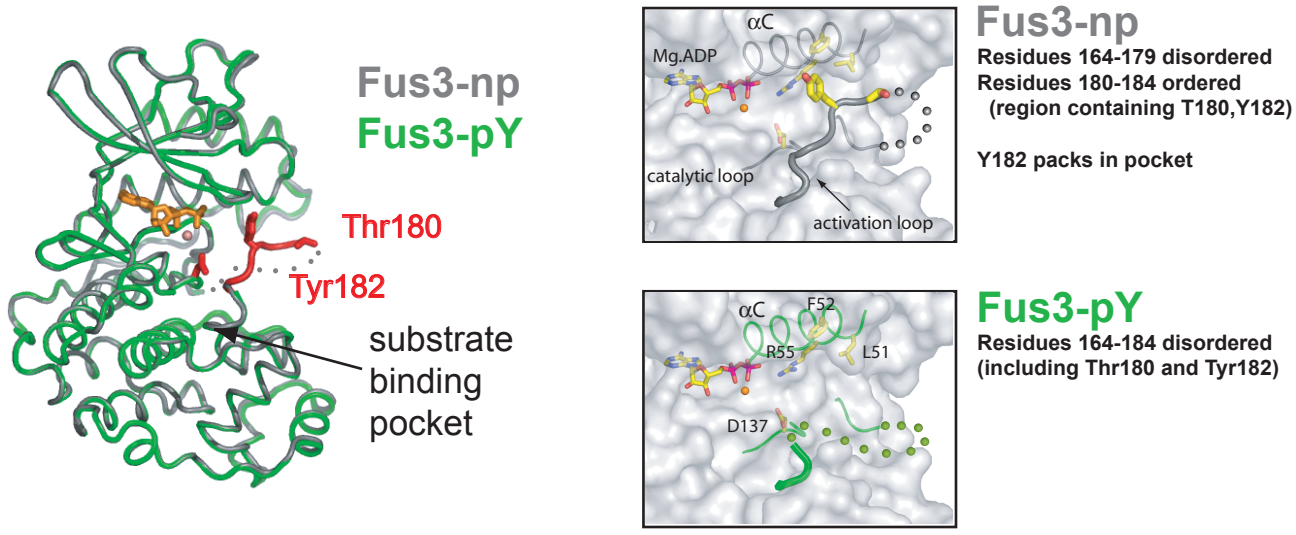

Figure S5. Structure of Fus3-pY compared to non-phosphorylated form.
In the non-phosphorylated Fus3 (Fus3-np) crystal structure, the N-terminal part of the activation segment (residues 164-179) is invisible, indicating the flexible nature of this region (depicted with dots). The C-terminal part of the phosphorylation lip (residues 180-185, shown in red), however, is clearly structured and positioned in the substrate binding pocket. In contrast, this region of the activation loop is invisible and more flexible in the Fus3-pY crystal structure. Comparison of the Fus3-np crystal structure with that of Fus3-pY reveals no other differences apart from a more open substrate binding pocket. Fus3-pY and Fus3-np crystallized under identical conditions in the same space group with identical cell dimensions. Moreover, both proteins bind Mg-ADP in the nucleotide binding pocket, and their structures were solved to 2.1 and 1.8 Å resolution, respectively (**Table S3**) (*S1*). (The slightly lower resolution of the Fus3-pY structure could not account for higher flexibility, and in turn for greater accessibility of the substrate binding pocket, because parts of the protein with higher crystallographic B factors are clearly visible in the electron density.) The close-up views around the catalytic loop (with D137) and the activation loop (with T180 and Y182) show that the Tyr182 fits into a pocket outlined by residues at the N-terminal part of αC (or α1). A bulkier phosphotyrosine side chain could not occupy the same position due to steric constraints.
CONCLUSION: These findings suggest a simple activation mechanism for Fus3: phosphorylation on Tyr182 renders the whole activation loop more flexible and opens access to a preassembled active site for substrates. The presence of Ste5_pep facilitates this process.

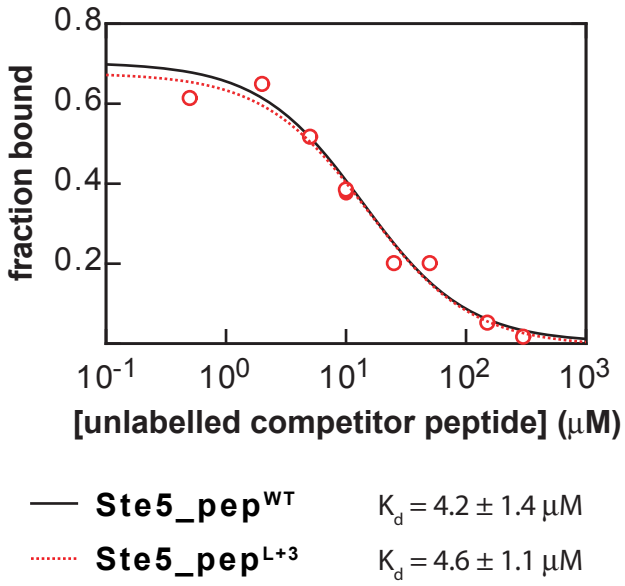

Ste5_pep^{WT}: TPVERQTIYSQAPSLNPNLILAAPPKERNQ
Ste5_pep^{L+3}: TPVERQTIYSQAPSSSSLNPNLILAAPPKERNQ

Figure S6. A three amino acid insertion into the Ste5_pep linker region does not alter binding affinity for Fus3.
Binding of Ste5_pep^{L+3} (amino acid boundaries 287-316) to Fus3 was measured by competition fluorescence polarization experiments and compared with that of Ste5_pep^{WT} (**Fig. S2**). Both peptides bind Fus3 with equal affinity within error (Ste5_pep^{L+3}: open red circles, dotted red line; Ste5_pep^{WT}: solid line, data points omitted here for clarity, but see **Fig. S2**).
CONCLUSION: Lengthening the linker between site A and site B of Ste5_pep (**Fig. 2A**) does not alter its binding affinity for Fus3. Thus, the reduction in enhancement of Fus3 autophosphorylation by this peptide variant (**Fig. 3E**) is not simply due to reduced binding.

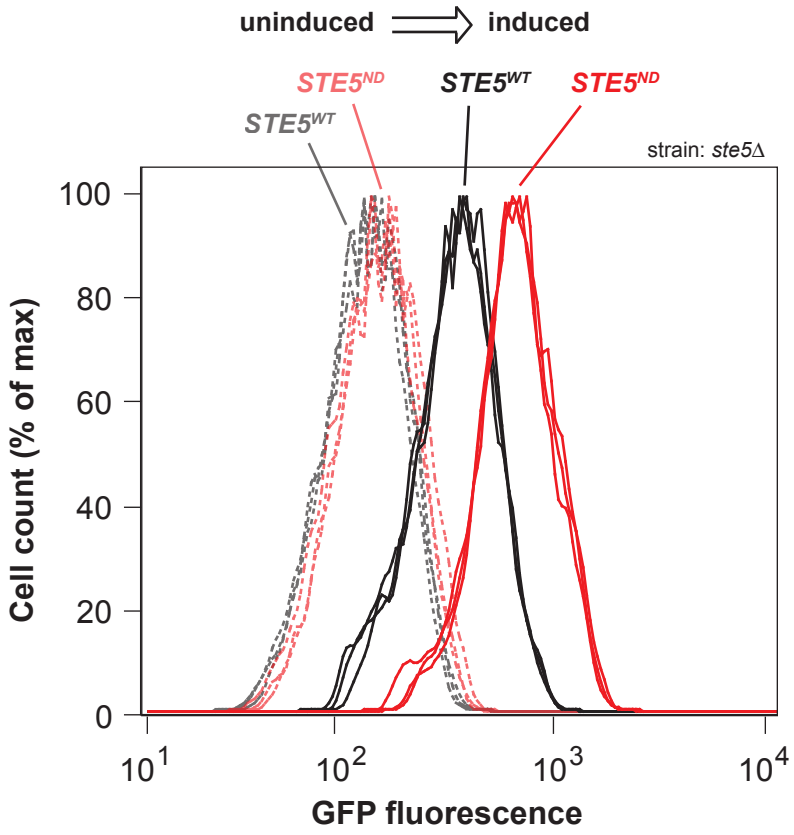

Figure S7. Flow cytometry histograms of Ste5 variants before and after alpha factor treatment.

The CB011 strain (see **Table S2**), transformed with a plasmid encoding either *STE5*^{WT} or *STE5*ND, was treated with a saturating dose of α-factor for 110 minutes. Population distributions of Fus1-GFP expression were detected by flow cytometry. Data from different experiments with three independent transformants are shown (dashed black = *STE5*^{WT}, no α-factor; dashed red = *STE5*ND, no α-factor; solid black = *STE5*^{WT}, 200 nM α-factor; solid red = *STE5*ND, 200 nM α-factor).

CONCLUSION: Flow cytometric detection of Fus1-GFP expression gives a reproducible measure of the response to α-factor. *STE5*^{WT} and *STE5*ND populations clearly have distinct responses to α-factor, and the difference between these populations is much greater than the difference between independent transformants of the same allele.

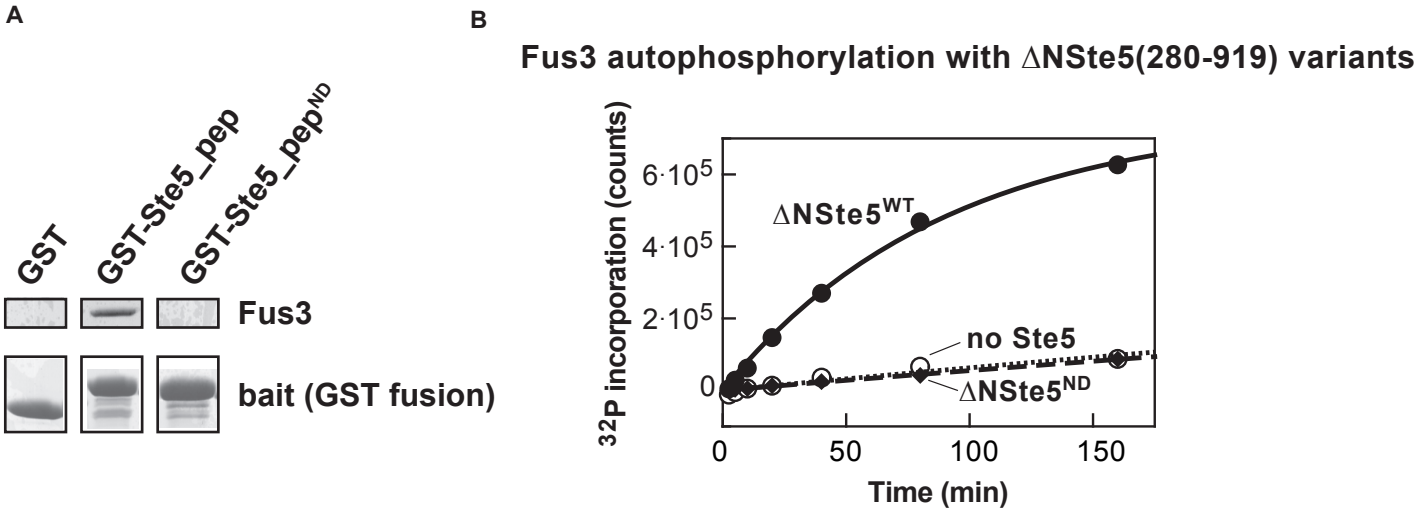

Figure S8. Ste5ND mutations disrupt binding and allosteric activation of Fus3.
(A) Fus3 associates by GST pulldown with the extended Ste5_pep^{WT} (amino acids 280-321) but not with the non-docking variant Ste5_pepND (**Fig. 4B**). GST fusions ("bait") and Fus3 are both shown by Coomassie blue staining. **(B)** Fus3 autophosphorylation is also enhanced by a large fragment of Ste5 containing the binding domains for all MAPK module components, which we call ΔNSte5 (amino acids 280-919, the largest fragment of Ste5 that we were readily able to express and purify). However, a variant of this protein harboring the ND mutations in the Ste5_pep region that binds Fus3 (ΔNSte5ND) does not enhance auto-acitivation of Fus3. Data from an autoradiogram were quantified and plotted along with a fit to an equation describing unimolecular autophosphorylation kinetics (Fus3 alone: open circles, dashed line; ΔNSte5^{WT}: filled circles, solid line; ΔNSte5ND: filled diamonds, dotted line).
CONCLUSION: The interface between Fus3 and Ste5_pep observed in the crystal structure is functionally relevant for Fus3 binding and is both necessary and sufficient for enhancement of Fus3 autophosphorylation.

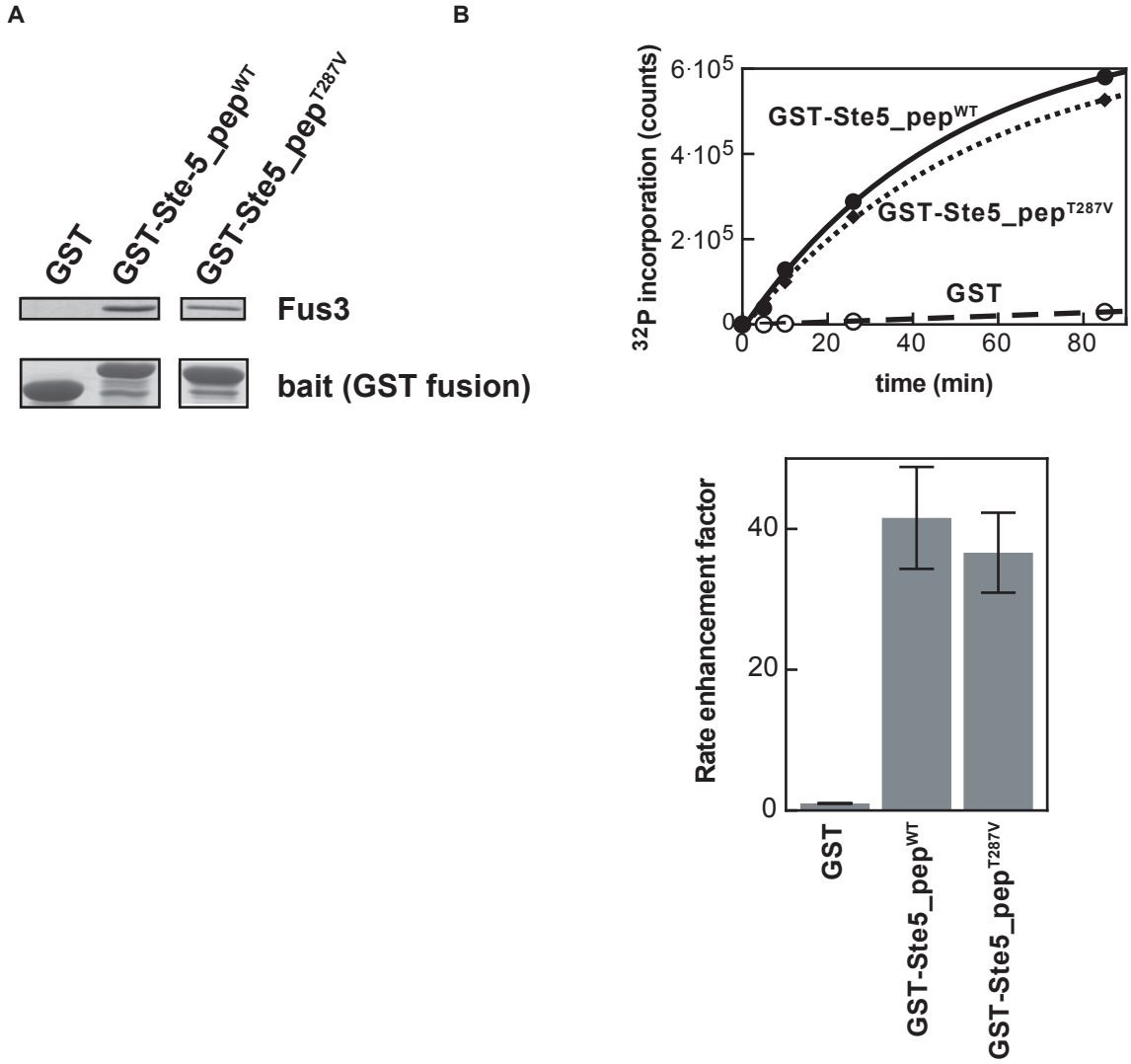

Figure S9. Ste5_pep^{T287V} mutation does not prevent binding or allosteric activation of Fus3.

(A) Thr287 is not required for the interaction between Fus3 and Ste5_pep. GST pull-downs demonstrate that both wild-type and T287V variants of the extended Ste5_pep (amino acids 280-321) interact with Fus3. **(B)** Thr287 is not required for enhanced autophosphorylation of Fus3 by Ste5_pep. Data from an autoradiogram were quantified and plotted along with a fit to an equation describing unimolecular activation kinetics (top panel). Relative rates of autophosphorylation obtained from the fits are plotted in the bottom panel.

CONCLUSION: Thr287, the primary phosphoacceptor residue in Ste5_pep (**Fig. 5A**), is not required for Fus3 binding or enhanced autophosphorylation. Therefore the increased pathway output seen with the T287V point mutants (**Fig. 5B**) likely has a different underlying cause than the non-docking mutants that block Fus3 binding and auto-activation enhancement.

Table S1: Plasmids used in this study

plasmid	parent vector	promoter	Description
vMG110	pRS314*	Ste7 native	$Ste7^{WT}$-myc_{13}
vMG111	pRS314	Ste7 native	$Ste7^{ND1}$-$myc_{13}^{(R9A,R10A,L15A,L17A)}$
vMG112	pRS314	Ste7 native	$Ste7^{ND2}$-$myc_{13}^{(R62A,R63A,L69A,L71A)}$
vMG113	pRS314	Ste7 native	$Ste7^{ND1,ND2}$-myc_{13}
pSH95	pRS316†	Ste5 native	$Ste5^{WT}$
pRB200	pRS316	Ste5 native	$Ste5^{ND(Q292A,I294A,Y295A,L307A,P310A,N315A)}$
pRB215	pRS316	Ste5 native	$Ste5^{T287V}$
pRB217	pRS316	Ste5 native	$Ste5^{ND,T287V}$
pRB128	pGEX 4T-1‡		GST-Ste5_pep^{WT}(280-321)
pRB140	pGEX 4T-1		GST-Ste5_pep^{T287V}(280-321)
pRB144	pGEX 4T-1		GST-Ste5_pep^{ND}(280-321)
pETARA S5	pET19b§		GST-Ste5_pep^{WT}(288-316)
pETARA S5 L-3	pET19b		GST-Ste5_pep^{L-3}(288-316 Δ300-302)
pETARA S5 L-2	pET19b		GST-Ste5_pep^{L-2}(288-316 Δ300 Δ302)
pETARA S5 L-1	pET19b		GST-Ste5_pep^{L-1}(288-316 Δ300)
pETARA S5 L+1	pET19b		GST-Ste5_pep^{L+1}(288-300-Ser-301-316)
pETARA S5 L+2	pET19b		GST-Ste5_pep^{L+2}(288-300-Ser_2-301-316)
pETARA S5 L+3	pET19b		GST-Ste5_pep^{L+3}(288-300-Ser_3-301-316)
pBH4 Fus3	pET19b		His_6-[TEV site]-$Fus3^{WT}$
pBH4 Fus3VF	pET19b		His_6-[TEV site]-$Fus3^{T180V,Y182F}$
pBH4 Fus3T180V	pET19b		His_6-[TEV site]-$Fus3^{T180V}$
pBH4 Fus3Y182F	pET19b		His_6-[TEV site]-$Fus3^{Y182F}$
pETARA dNSte5	pET19b		GST-$Ste5^{WT}$(280-919)-His_6
pETARA dNSte56A	pET19b		GST-$Ste5^{ND}$(280-919)-His_6
pFastBac M Ste7EE	pFastBac‖		GST-$Ste7^{S259E,T363E}$-His_6

*pRS314 is a low-copy yeast vector (CEN/ARS origin, *TRP1*)
†pRS316 is a low-copy yeast vector (CEN/ARS origin, *URA3*)
‡pGEX 4T-1 is a bacterial vector for expression of GST fusion proteins (Amersham)
§pET-19b is a bacterial expression vector (Novagen)
‖pFastBac is an insect cell expression vector (Invitrogen)

Table S2: Yeast strains used in this study

Strain	*Description*
CB011	W303 *MAT**a**, ste5::KanR, bar1::NatR, far1*Δ*, mfa2::pFus1-GFP, his3, trp1, leu2, ura3*
CB006Δste5	W303 *MAT**a**, ste5*Δ*, bar1::NatR, mfa2::pFus1-GFP, his3, trp1, leu2, ura3*
MG40	W303 *MAT**a**, ste7::HIS3, bar1::NatR, far1*Δ*, mfa2::pFus1-GFP, trp1, leu2, ura3*

Table S3. Crystallographic data and refinement statistics

	Fus3^{VF} *uncomplexed*	*Fus3*^{VF}*/ Ste5_pep*	*Fus3-pY*
Space group	$P2_12_12_1$	$P2_12_12_1$	$P2_12_12_1$
Resolution range (Å)	50–2.85	50–1.9	50–2.1
No. of data	19,082	69,007	18,096
Completeness (%)[a]	94.1	95.3	97.3
Multiplicity	3.4	4.4	3.0
R_{sym}[*,†]	7.4 (18.9)	7.0 (50.0)	9.0 (34.6)
$I / \sigma I$[*]	13.5 (3.9)	15.3 (2.4)	10.7 (2.2)
R_{cryst}[‡]	20.9	20.1	21.1
R_{free}[‡]	28.5	23.4	26.0
No. of atoms	5363	6066	2810
H_2O	45	480	100
RMSD Bonds (Å)	0.011	0.011	0.013
RMSD Angle (°)	1.6	1.5	1.6

[*]Values in parentheses are for the highest resolution shell.

[†]$R_{sym} = \Sigma_{hkl}\Sigma_i |I_i(hkl) - \langle I(hkl)\rangle| / \Sigma_{hkl}\Sigma_I I_i(hkl)$.

[‡]R_{cryst} and $R_{free} = |\Sigma F_{obs} - F_{calc}| / \Sigma F_{obs}$; R_{free} is calculated with 10% of the data that were not used for refinement.

Supplemental References:

S1. A. Remenyi, M. C. Good, R. P. Bhattacharyya, W. A. Lim, *Mol Cell*, in press.
S2. B. Z. Harris, B. J. Hillier, W. A. Lim, *Biochemistry* **40**, 5921 (2001).
S3. Z. Otwinowski, W. Minor, *Methods Enzymology* **A276**, 307 (1997).
S4. J. Navaza, *Acta Crystallogr A* **50**, 157 (1994).
S5. T. A. Jones, J. Y. Zou, S. W. Cowan, Kjeldgaard, *Acta Crystallogr A* **47**, 110 (1991).
S6. A. T. Brunger *et al.*, *Acta Crystallogr D Biol Crystallogr* **54**, 905 (1998).
S7. W. V. Bienvenut *et al.*, *Proteomics* **2**, 868 (2002).
S8. M. Peter, A. Gartner, J. Horecka, G. Ammerer, I. Herskowitz, *Cell* **73**, 747 (1993).
S9. V. L. MacKay *et al.*, *Proc Natl Acad Sci U S A* **85**, 55 (1988).
S10. M. A. Poritz, S. Malmstrom, M. K. Kim, P. J. Rossmeissl, A. Kamb, *Yeast* **18**, 1331 (2001).
S11. K. Y. Choi, B. Satterberg, D. M. Lyons, E. A. Elion, *Cell* **78**, 499 (1994).
S12. A. M. Falick, unpublished data.
S13. R. P. Bhattacharyya, A. Remenyi, W. A. Lim, unpublished data.